Bioconjugate Chemistry

pubs.acs.org/bc

Article

Helix-Stabilized Cell-Penetrating Peptides for Delivery of Antisense Morpholino Oligomers: Relationships among Helicity, Cellular Uptake, and Antisense Activity

Hiroyuki Takada, Keisuke Tsuchiya, and Yosuke Demizu*

Cite This: *Bioconjugate Chem.* 2022, 33, 1311−1318

Read Online

ACCESS | Metrics & More | Article Recommendations | Supporting Information

ABSTRACT: The secondary structures of cell-penetrating peptides (CPPs) influence their properties including their cell-membrane permeability, tolerability to proteases, and intracellular distribution. Herein, we developed helix-stabilized arginine-rich peptides containing α,α-disubstituted α-amino acids and their conjugates with antisense phosphorodiamidate morpholino oligomers (PMOs), to investigate the relationships among the helicity of the peptides, cellular uptake, and antisense activity of the peptide-conjugated PMOs. We demonstrated that helical CPPs can efficiently deliver the conjugated PMO into cells compared with nonhelical CPPs and that their antisense activities are synergistically enhanced in the presence of an endosomolytic reagent or an endosomal escape domain peptide.

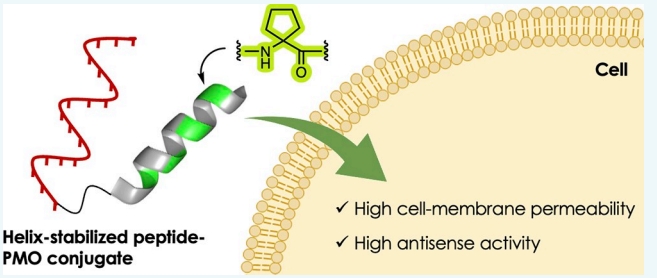

INTRODUCTION

Peptide foldamers are oligopeptides that adopt well-defined secondary structures such as helix, β-sheet, or turn structures.[1−3] The conformations of peptides are known to influence their various properties including their cell-membrane permeability, binding affinity to proteins, and tolerability to proteases. Indeed, for the design of cell-penetrating peptides (CPPs), it is attempted to control secondary structures by macrocyclization[4] or incorporation of α,α-disubstituted α-amino acids (dAAs),[5−7] β-amino acids,[8] γ-amino acids,[9] proline,[10] and cross-linked side chains,[11−13] among other methods.[14] Many studies in the past few decades revealed that CPPs with rigid structures have high cell-membrane permeability compared with conventional CPPs such as TAT, Penetratin, or oligoarginine with random structures. For example, we previously demonstrated that introducing 2-aminoisobutyric acid (Aib), the simplest dAA, into the oligoarginine sequence induced the formation of a helical structure and the enhancement of cellular uptake (Figure 1).[6] Similarly, we developed a cationic dAA with a guanidino side chain, 4-amino-1-(3-guanidinopropanoyl)-piperidine-4-carboxylic acid (Api^{C2Gu}), and the peptide containing the Api^{C2Gu} residues formed a stable helical structure and exhibited higher cell permeability than that of a nonaarginine (R9) peptide.[7] Namely, the stabilization of helical structures of cationic CPPs results in the enhancement of their cell permeability.

CPPs are a powerful tool for intracellular delivery of impermeable macromolecules such as antibodies, enzymes, and oligonucleotides.[15,16] In terms of the delivery of antisense oligonucleotides, several successful studies have been reported on conjugates of cationic CPPs with phosphorodiamidate morpholino oligomers (PMOs). Moulton et al. demonstrated that the conjugate of the R9 peptide with PMOs showed greater cell permeability and antisense activity compared with the naked PMO.[17] Furthermore, they identified a novel CPP Bpep, where 6-aminohexanoic acids (Ahx) are inserted into oligoarginine as C6 spacers, and its conjugate with PMOs possesses higher potency than that of the R9 conjugate.[18,19] Gait and Wood et al. developed a PMO internalizing peptide (Pip) series and its PMO conjugates by introducing a partial moiety of Penetratin into the Bpep sequence. Their peptide-conjugated PMOs (PPMOs) showed higher exon-skipping efficacy in mdx mice, a model of Duchenne muscular dystrophy, compared with the naked PMO.[20] By comparison, there are few studies where peptide foldamers are used for the delivery of PMOs. Wolfe and Fadzen et al. synthesized cyclic arginine-rich peptides by using perfluoroarenes and evaluated the antisense activities of the corresponding PPMOs.[21] However, the relationships of their secondary structures with cellular uptake and antisense activity are not well-understood. Therefore, we designed and synthesized helical CPPs by introducing dAAs into the R9 peptide and investigated their

Received: April 24, 2022
Revised: June 9, 2022
Published: June 23, 2022

https://doi.org/10.1021/acs.bioconjchem.2c00199
Bioconjugate Chem. 2022, 33, 1311−1318

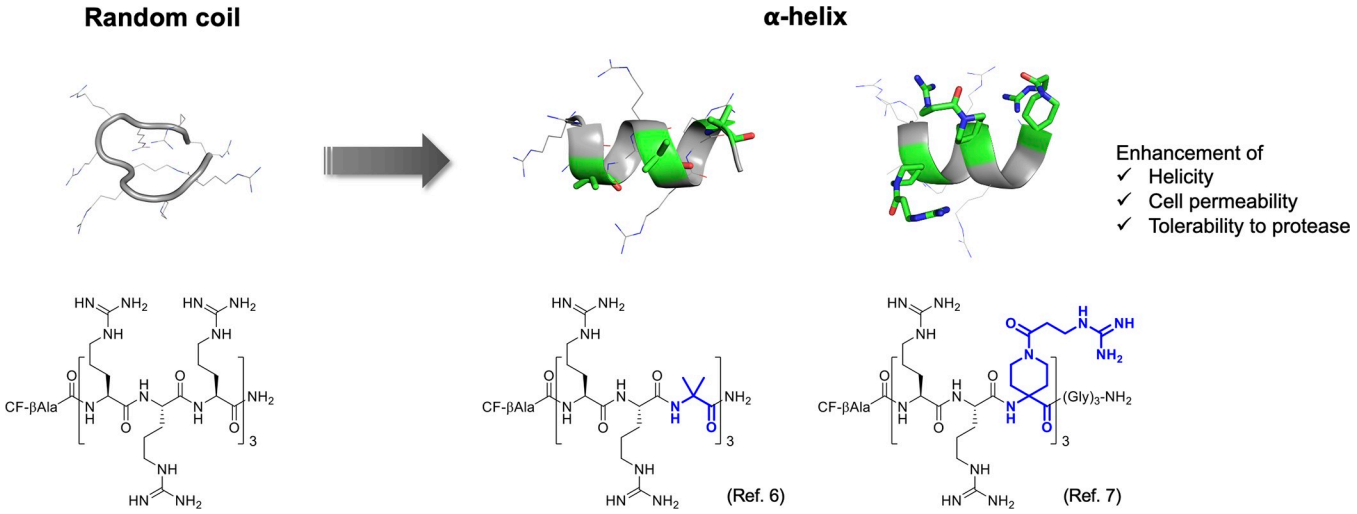

Figure 1. Development of helix-stabilized cell-penetrating peptides by introducing α,α-disubstituted α-amino acids. CF = 5(6)-carboxyfluorescein.

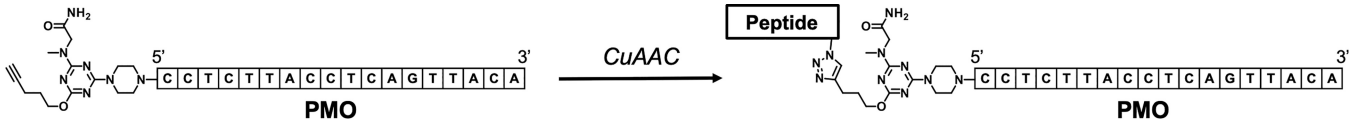

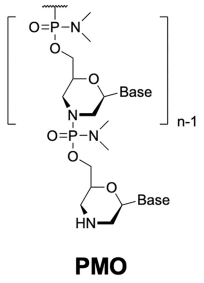

Conjugate	Peptide	Sequence of peptide
1	-	-
2	**2a**	RRRRRRRRR
3	**3a**	RRX^{1}RRX^{1}RRX^{1}RRX^{1}RZ
4	**4a**	RRX^{2}RRX^{2}RRX^{2}RRX^{2}RZ
5	**5a**	RRX^{3}RRX^{3}RRX^{3}RRX^{3}RZ
6	**6a**	RRX^{4}RRX^{4}RRX^{4}RRX^{4}RZ
7	**7a**	RrX^{3}RrX^{3}RrX^{3}RrX^{3}RZ
8	**8a**	rrX^{3}rrX^{3}rrX^{3}rrX^{3}rZ
5-F	**5a-F**	CF-B-RRX^{3}RRX^{3}RRX^{3}RRX^{3}RZ
7-F	**7a-F**	CF-B-RrX^{3}RrX^{3}RrX^{3}RrX^{3}RZ
8-F	**8a-F**	CF-B-rrX^{3}rrX^{3}rrX^{3}rrX^{3}rZ
9	**9a**	GFWFG-Ahx-rrX^{3}rrX^{3}rrX^{3}rrX^{3}rZ

X^1 = Aib
X^2 = Ac$_4$c
X^3 = Ac$_5$c
X^4 = Ac$_6$c
Z = Lys(N$_3$)

Figure 2. Structures of the PPMOs. Peptide sequences are described from the N- to C-terminus. r = D-arginine, B = β-alanine, CF = 5(6)-carboxyfluorescein, and Ahx = 6-aminohexanoic acid.

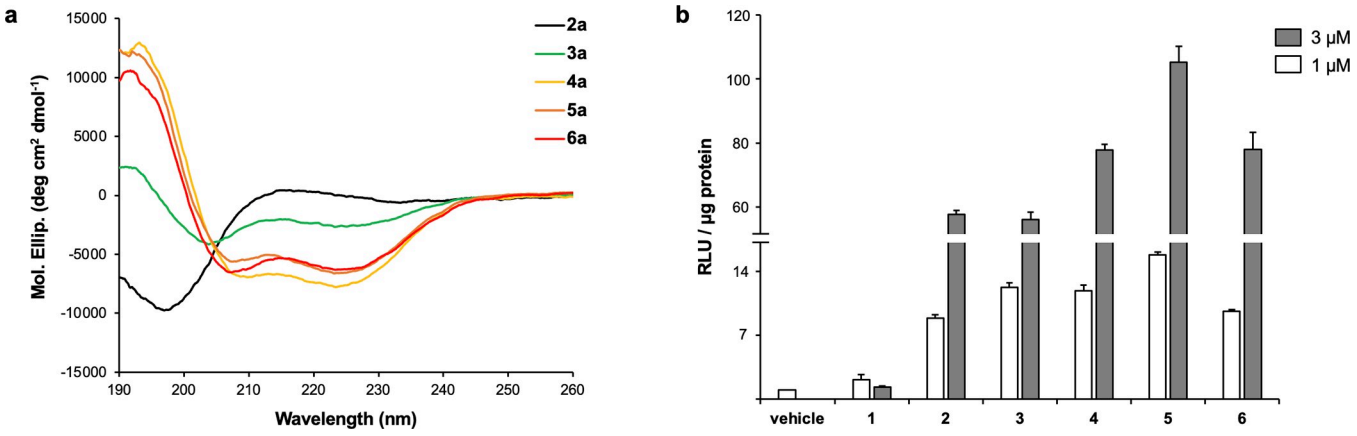

Figure 3. Structure−activity relationships of the PPMOs. (a) CD spectra of peptides **2a**−**6a** in 20 mM phosphate buffer (pH 7.4). The peptide concentration was 100 μM. (b) Antisense activities of the PMO **1** and PPMOs **2**−**6**. HeLa 705 cells were treated with 1 or 3 μM of the compounds for 24 h. Antisense activities are indicated as relative light units (RLU) per microgram of protein. Data represent the mean ± SEM of four samples.

https://doi.org/10.1021/acs.bioconjchem.2c00199
Bioconjugate Chem. 2022, 33, 1311−1318

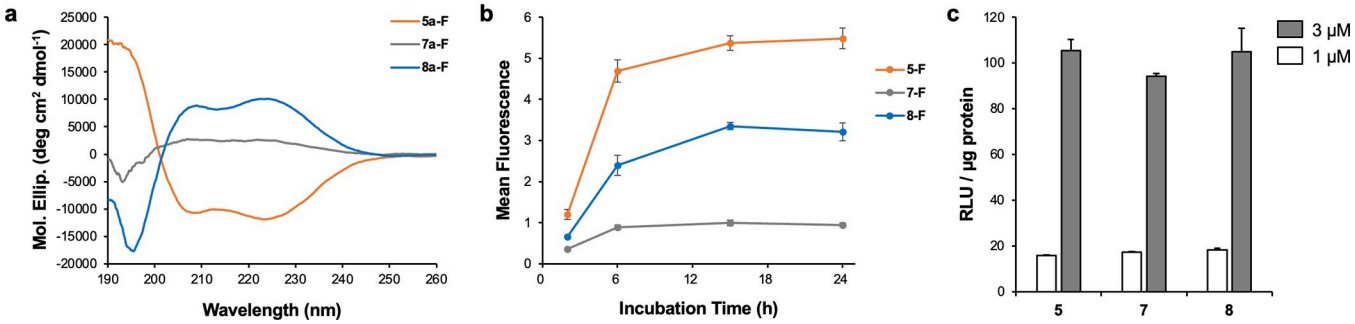

Figure 4. Relationships among the helicity of the peptides, cellular uptake, and antisense activity of the PPMOs. (a) CD spectra of **5a-F**, **7a-F**, and **8a-F** in 20 mM phosphate buffer (pH 7.4). The peptide concentration was 100 μM. (b) Cellular uptake of **5-F**, **7-F**, and **8-F**. HeLa 705 cells were treated with 1 μM of the conjugates for 2, 6, 15, and 24 h followed by the flow cytometry measurement. Data represent the mean ± SEM of six samples. (c) Antisense activities of **5**, **7**, and **8**. HeLa 705 cells were treated with 1 or 3 μM of the conjugates for 24 h. Antisense activities are indicated as relative light units (RLU) per microgram of protein. Data represent the mean ± SEM of four samples.

effects on the cell permeability and antisense activity of the corresponding PPMOs. In this study, we demonstrate that helix-stabilized CPPs can efficiently deliver the conjugated PMO inside cells, leading to an increase in the antisense activity in the presence of endosomal escape enhancers such as chloroquine or an endosomal escape domain peptide.

RESULTS AND DISCUSSION

First, we designed helical CPPs containing dAAs **3a**–**6a**, where four residues of Aib, 1-aminocyclobutanecarboxylic acid (Ac_4c), 1-aminocyclopentanecarboxylic acid (Ac_5c), or 1-aminocyclohexanecarboxylic acid (Ac_6c) were introduced into the R9 peptide **2a** (Figure 2). The peptides were synthesized by Fmoc solid-phase peptide synthesis. They have a Lys(N_3) residue at the C-terminus for the conjugation reaction with PMOs. The secondary structures of **2a**–**6a** were analyzed by circular dichroism (CD) spectroscopy in 20 mM phosphate buffer (Figure 3a). Expectedly, the peptide **3a** containing Aib exhibited negative maxima at around 203 and 225 nm, indicating that **3a** should form a right-handed α-helical structure, while the R9 peptide **2a** showed a random-coil-like CD spectrum with a negative maximum at 196 nm and a weak positive maximum at 214 nm. Furthermore, **4a**–**6a** containing cyclic dAAs had negative maxima at around 208 and 223 nm, and the intensities of negative maxima increased compared with **3a**. This suggested that the helical structures of **4a**–**6a** were highly stabilized by introducing cyclic dAAs. Next, the obtained peptides **2a**–**6a** were conjugated with PMOs by copper-catalyzed azide–alkyne cycloaddition (CuAAC) to afford the corresponding PPMOs **2**–**6**, respectively (Figure 2).

For evaluation of the antisense activities of the obtained PPMOs, we used the HeLa 705 splicing assay system developed by the Kole group.[22] HeLa 705 cells were stably transfected with a luciferase gene, but its protein expression was disturbed by the insertion of a mutation sequence derived from intron 2 of the human β-globin gene. The employed PMO was designed to hybridize to the mutation region and induce splicing modulation resulting in the removal of the aberrant motif from luciferase mRNA and the correct protein expression. Therefore, in this assay system, the nuclear delivery and antisense activity of PPMOs can be evaluated by measuring the luminous signals of treated cells. The cultured HeLa 705 cells were treated with the naked PMO **1** and PPMOs **2**–**6** at 1 and 3 μM, and then, the luciferase expression levels in the treated cells were evaluated (Figure 3b). As previously reported,[17] the R9 peptide conjugate **2** showed a dramatic increase in antisense activity compared with the naked PMO **1** of which the luminous intensity was similar to that of the vehicle controls even at 3 μM. The antisense activity of the conjugate **3** containing the Aib residues was higher than that of the R9 conjugate **2** at 1 μM, although they were comparable at 3 μM. By comparison, the conjugate **4** containing Ac_4c showed greater potency relative to **2** at both 1 and 3 μM. Furthermore, the conjugate **5**, where the cyclobutyl rings of **4** were replaced with cyclopentyl rings, was more potent than **4**, while the conjugate **6** containing cyclohexyl rings was comparable to **4**. Taken together, helical CPP conjugates **3**–**6** showed higher antisense activities compared with the R9 conjugate **2**, and among them, the conjugate **5** containing Ac_5c exhibited the best splicing correction efficacy in a dose-dependent manner. However, it should be considered that reverse-phase HPLC analyses of the peptides indicated that helical peptides **3a**–**6a** were more lipophilic than the R9 peptide **2a** (Figure S3). Abes et al. reported the structure–activity relationships of $(R\text{-}X\text{-}R)_4$-PMO conjugates, where X represents linear hydrocarbon spacers, and demonstrated that a PPMO with a C6 spacer (X = Ahx) exhibited a higher antisense activity than that of a PPMO with a C2 or C4 spacer (the rank order was C6 > C4 > C2) although it was not well-understood which factor had a large impact on their antisense activities, the length or lipophilicity of spacers.[23] Therefore, not only the helicities but also the lipophilicities of **3a**–**6a** could contribute to the enhancement of the antisense activity of PPMOs **3**–**6**. It should be noted that the cytotoxicity of the conjugate **5** was evaluated, and as indicated by the results, **5** showed minimal effects on the cell viability (>90% cell viability) at 1 and 3 μM (Figure S1).

With the potent conjugate **5** in hand, we investigated the relationships among the helicity of the peptides, cellular uptake, and antisense activity of the PPMOs. The peptide **5a** forms a right-handed α-helix because it is composed of L-amino acids [Arg and Lys(N_3)] and achiral Ac_5c. If these L-amino acids are substituted with D-amino acids, then an inversion of the screw sense should be induced, resulting in a left-handed α-helical structure. Furthermore, mixing L- and D-amino acids should lead to a decrease in helicity because both directional characteristics offset each other. Thus, we prepared peptides **7a** and **8a**, stereoisomers of **5a**, which are composed of L- and D-Arg or only D-Arg, respectively, to compare derivatives where the atomic compositions are equivalent but the helicities are different. Additionally, the fluorescein-labeled peptides **5a-F**,

https://doi.org/10.1021/acs.bioconjchem.2c00199
Bioconjugate Chem. 2022, 33, 1311–1318

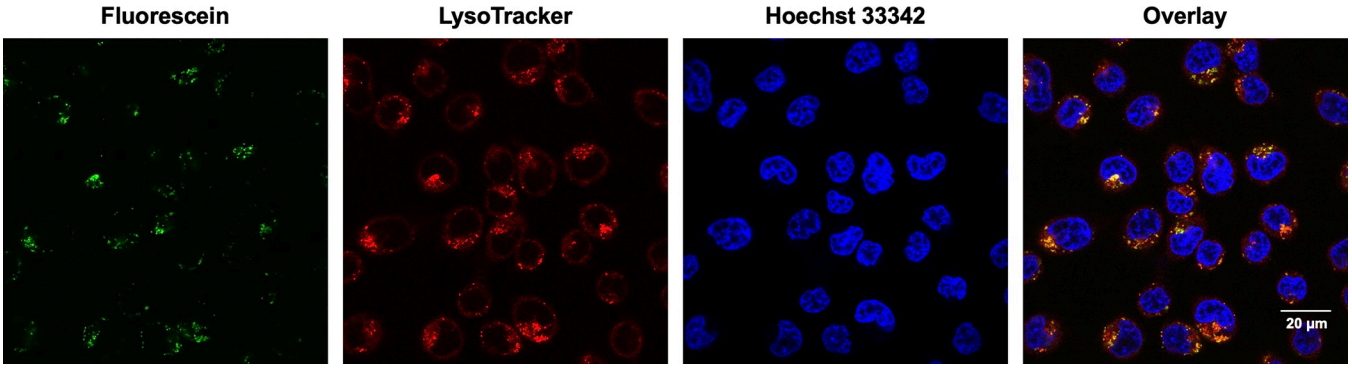

Figure 5. Confocal microscopy images of HeLa 705 cells treated with 1 μM PPMO **5-F** for 6 h. Nuclei and endosomes/lysosomes were stained by Hoechst 33342 and LysoTracker Red, respectively. The confocal microscopy observations were performed with a 100× objective lens.

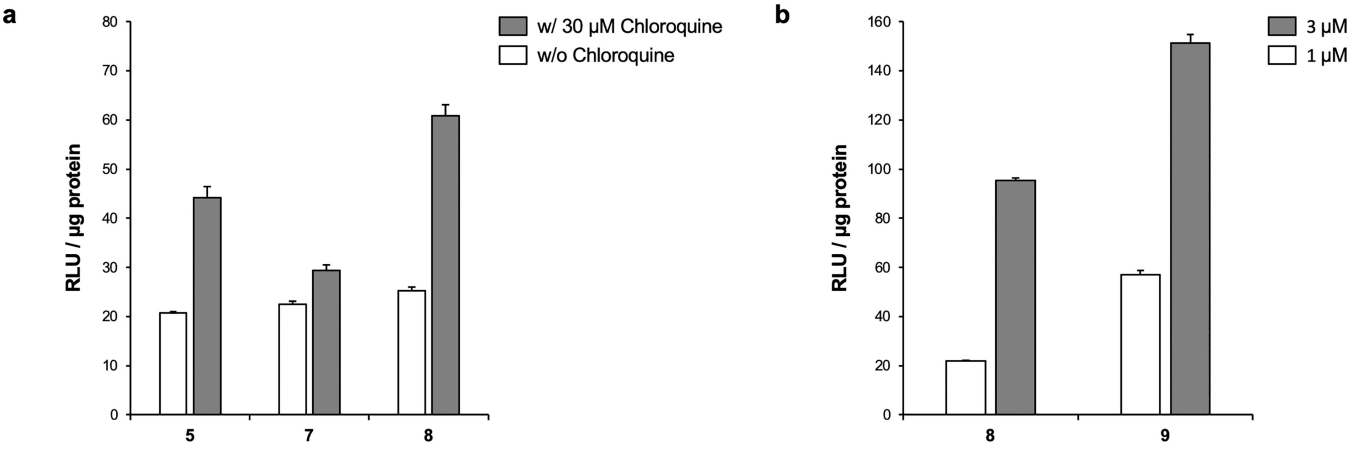

Figure 6. Antisense activities of PPMOs in the presence of an endosomolytic reagent or an endosomal escape domain peptide. (a) HeLa 705 cells were treated with 1 μM of **5**, 7, and **8** for 24 h in the presence or absence of 30 μM chloroquine. (b) HeLa 705 cells were treated with 1 or 3 μM of **8** and **9** for 24 h. Antisense activities are indicated as relative light units (RLU) per microgram of protein. Data represent the mean ± SEM of four samples.

7a-F, and **8a-F** were synthesized to evaluate the cellular uptake of the PPMOs. First, the secondary structures of **7a-F** and **8a-F** were compared with **5a-F** by CD spectroscopy (Figure 4a). The peptide **5a-F** exhibited a right-handed α-helix-like spectrum with negative maxima at around 208 and 223 nm, which was similar to that of nonlabeled **5a**. By comparison, a dramatic decrease in signal intensities was observed for the heterochiral peptide **7a-F**. This result should come about because there is no preference for a specific screw sense for the mixture of five L-Arg and four D-Arg. Expectedly, **8a-F** containing only D-Arg showed an almost mirror-image spectrum compared with that for **5a-F**, where the positive maxima were around 208 and 223 nm. However, the molar ellipticity of **8a-F** was slightly lower than that of **5a-F** (approx. 0.8-fold relative to **5a-F**), which might be because **8a-F** contains C-terminal L-Lys(N_3), and hence, it is not fully composed of D-amino acids.

Next, we synthesized PPMOs **5-F**, **7-F**, and **8-F** by using the fluorescein-labeled peptides. The cellular uptake of **5-F**, **7-F**, and **8-F** in HeLa 705 cells was compared by flow cytometry (Figure 4b). The cells were treated with 1 μM of each fluorescent PPMO for 2, 6, 15, and 24 h, and then, the intracellular fluorescence intensities were evaluated. As a result, the helical CPP conjugate **5-F** penetrated the cell membrane more efficiently than the nonhelical CPP conjugate **7-F** (approx. 5-fold higher after 15 h). It was previously reported that the helical oligoarginine peptide containing the Aib residues showed higher cellular uptake than that of the corresponding heterochiral isomer depending on the difference of the helicities.[6] Our results demonstrated that stabilizing the helical structure of arginine-rich CPPs enhances the cell permeability of not only the peptides themselves but also the PPMOs. To our knowledge, this is the first time that the correlation between the helicities and cell permeabilities of PPMOs has been clarified by using stereoisomers. It is noteworthy that the lipophilicities of **5a-F**, **7a-F**, and **8a-F** are thought to be comparable because their retention times from reverse-phase HPLC analyses were similar (Figure S3). Although **8-F** was also taken up by cells more efficiently than **7-F**, it was not taken up as efficiently as **5-F**. This might be because the helicity of **8a-F** is lower than that of **5a-F**. Next, to confirm whether the observed intracellular amounts of the PPMOs correlate with the antisense activities, we measured the splicing correction efficacy of the cells treated with **5**, **7**, and **8**. Contrary to the results of the cellular uptake assay, all PPMOs exhibited comparable antisense activities (Figure 4c). We assumed that it was because of endosomal entrapment that the efficient cellular uptake of **5** and **8** was not reflected in their splicing correction efficacy.

Previous studies reported that arginine-rich PPMOs are internalized into cells by energy-dependent mechanisms such as clathrin-mediated endocytosis, caveolae-mediated endocy-

https://doi.org/10.1021/acs.bioconjchem.2c00199
Bioconjugate Chem. 2022, 33, 1311−1318

tosis, and macropinocytosis.[18,24,25] After being taken up, the internalized PPMOs are localized at endosomal vesicles; hence, they need to escape from the endosomes and move into the nuclei for the splicing correction. Therefore, it was suggested that the low efficiency of the endosomal escape of the helical CPP conjugates **5** and **8** limited their antisense activities to levels comparable to that of the nonhelical CPP conjugate **7**. In fact, it was previously reported that the R9-PMO conjugate exhibited a lower antisense activity than that of the (R-Ahx-R)$_4$-PMO conjugate despite its higher cellular uptake than that of (R-Ahx-R)$_4$-PMO, which is considered to be attributed to the endosomal escape efficiency.[18,19]

The imaging data of cells treated with fluorescein-labeled PPMOs supported our hypothesis. In accordance with the results of flow cytometry, brighter green fluorescence was observed in the cells treated with **5-F** compared with the cells treated with **7-F** (Figure S2). However, the green fluorescence of **5-F** was distributed in a punctate pattern and colocalized with the endosome/lysosome marker LysoTracker Red, indicating that most of the internalized PPMOs remained within endosomes or lysosomes and did not reach the nucleus (Figure 5).

If endosomal entrapment limits the antisense activity of highly internalized PPMOs, then promoting their endosomal escape should improve the antisense activity. Thus, we compared the antisense activities of **5**, **7**, and **8** in the presence of chloroquine, which is known to be an endosomolytic reagent.[18] HeLa 705 cells were coincubated with each PPMO and 30 μM chloroquine for 24 h, and the luciferase expression levels were evaluated. Consequently, an increase in splicing correction efficacy was observed in all conjugate-treated groups compared with the case in the absence of chloroquine (Figure 6a). Furthermore, helical CPP conjugates **5** and **8** exhibited obviously higher antisense activities compared with **7** (approx. 1.5- and 2-fold higher, respectively) in the presence of chloroquine, suggesting a synergistic effect of efficient cellular uptake and cytosolic release. In particular, the D-isomer **8** was more potent than the L-isomer **5**, which might depend on the intracellular metabolic stability of the peptide moieties. It was previously revealed that PPMOs containing adjacent L-Arg residues can be quickly degraded by proteases inside cells despite the presence of unnatural spacer amino acids in the peptide sequence.[26] These results implied that the attached peptides might affect the intracellular behaviors of PPMOs, such as their endosomal escape and nuclear distribution. Finally, we designed the CPP **9a**, where a GFWFG fragment was conjugated at the N-terminus of **8a** via an *n*-hexyl linker, which is known as an endosomal escape domain (EED). Lönn et al. introduced the GFWFG moiety to TAT peptide-conjugated GFPβ11, which is a fragment of the β-strand of GFP, and demonstrated that the cytosolic distribution of TAT-GFPβ11 was enhanced when the GFWFG moiety was conjugated.[27] The synthesized **9a** was coupled with a PMO, and the resulting PPMO **9** was administrated to HeLa 705 cells. As a result, the CPP-EED conjugate **9** showed a higher splicing correction efficacy than that of **8** at both 1 and 3 μM (Figure 6b). Taken together, helical CPPs efficiently deliver the conjugated PMO inside cells, and combining them with endosomolytic reagents or peptides can synergistically increase the antisense activity.

CONCLUSIONS

In summary, we designed helix-stabilized arginine-rich peptides containing various dAAs to identify highly cell-permeable and potent PPMOs. Among them, the conjugate **5** containing Ac_5c residues exhibited the strongest antisense activity. Furthermore, the relationships among the helicity of the peptides, cellular uptake, and antisense activity of the PPMOs were investigated by using stereoisomers where the chirality of the Arg residues was altered. Consequently, it was found that helical CPPs can deliver the conjugated PMO inside cells more efficiently than nonhelical CPPs, but the antisense activities of the conjugates were comparable regardless of the cellular uptake amounts due to endosomal entrapment. However, coadministration of chloroquine, an endosomolytic reagent, synergistically improved the antisense activities of helical CPP conjugates **5** and **8**, suggesting that stabilizing the helical structure of CPPs is effective to enhance the antisense activity of PPMOs when their endosomal escape is promoted. We continue to optimize the structure of helical CPPs containing an EED such as the GFWFG moiety to discover more potent PPMOs.

EXPERIMENTAL SECTION

Peptide Synthesis. The designed peptides were synthesized by Fmoc solid-phase peptide synthesis with a Biotage Syro I synthesizer. Before starting the peptide synthesis, NovaPEG Rink amide resin (50 μmol) was soaked for 1 h in CH_2Cl_2. In each coupling reaction, Fmoc-protected amino acids or 5(6)-carboxyfluorescein (6 equiv), 1-[bis-(dimethylamino)methylene]-1*H*-benzotriazolium 3-oxide hexafluorophosphate (HBTU, 6 equiv), 1-hydroxybenzotriazole monohydrate (HOBt, 6 equiv), and *N*,*N*-diisopropylethylamine (DIPEA, 10 equiv) were used in DMF (4 mL). Coupling reactions were performed twice at 30 °C for 1 h. Deprotection of Fmoc groups was performed with 40% piperidine in DMF (3 mL) at 30 °C for 3 min and then 20% piperidine in DMF (3 mL) at 30 °C for 12 min. After the final deprotection, acetylation of the amino group at the N-terminus was conducted with acetic anhydride (0.4 mL), DIPEA (0.4 mL), and NMP (2 mL) at room temperature for 30 min. The resin was washed with CH_2Cl_2 and then suspended and stirred in 3 mL of cleavage cocktail (95% TFA, 2.5% water, and 2.5% triisopropylsilane) at room temperature for 3 h. The resin was removed by filtration, and the resulting TFA solution was evaporated to a small volume under a stream of N_2 gas. To the residue was added cold diethyl ether to precipitate the crude peptide. The crude peptide was purified by using a JASCO preparative HPLC system equipped with an Inertsil WP300 C18 column (250 mm × 20 mm ID, 5 μm, GL Sciences). Mobile phases A and B were 0.1% TFA in water and 0.1% TFA in acetonitrile, respectively. The fractions containing the target product were collected, concentrated in vacuo, and lyophilized to obtain the desired peptide. The purified peptides were analyzed by a JASCO analytical HPLC system equipped with an Inertsil WP300 C18 column (150 mm × 4.6 mm ID, 5 μm, GL Sciences). Mobile phases A and B were 0.1% TFA in water and 0.1% TFA in acetonitrile, respectively. MS identification was performed by a Shimadzu IT-TOF MS equipped with an electrospray ionization source.

Peptide-PMO Conjugation. Peptide-conjugated PMOs were synthesized and purified with reference to the reported

https://doi.org/10.1021/acs.bioconjchem.2c00199
Bioconjugate Chem. 2022, 33, 1311−1318

method.[28] A 5′-alkyne-modified PMO (5′-CCT CTT ACC TCA GTT ACA-3′) was purchased from Gene Tools (Oregon). To a solution of PMOs in water and DMSO (60:40) were added an azide-peptide (3 equiv), $CuSO_4$ (30 equiv), sodium ascorbate (30 equiv), and tris[(1-benzyl-1*H*-1,2,3-triazol-4-yl)methyl]amine (30 equiv). The reaction mixture was shaken at room temperature for 30 min. The mixture was purified by cation exchange column chromatography using a Shimadzu HPLC system equipped with a SOURCE 15S column (100 mm × 4.6 mm ID, Cytiva). Mobile phases A and B were 25 mM Na_2HPO_4 aq. and 1 M NaCl in 25 mM Na_2HPO_4 aq., respectively. Desalting of the obtained product was performed by using an Amicon Ultra 3K centrifugal filter device. The purity and MS spectra of obtained PPMOs were analyzed by a Waters LC−MS system (ACQUITY UPLC H-Class PLUS Bio with Xevo G2-XS TOF) equipped with a Proteonavi C4 column (50 mm × 2.0 mm ID, 5 μm, OSAKA SODA). Mobile phases A and B were 0.05% formic acid in water and 0.05% formic acid in acetonitrile, respectively. The purities of compounds for biological testing were >95%.

Circular Dichroism Spectroscopy. CD analysis of peptides was performed by using a JASCO CD spectrometer equipped with a 1.0 mm path length cell. Peptides were dissolved in 20 mM phosphate buffer solution (pH 7.4) at 100 μM concentrations. Spectra were recorded from 260 to 190 nm at 37 °C.

Cell Culture. The HeLa 705 cell line was obtained from the University of North Carolina Tissue Culture Facility. The cells were cultured in Dulbecco's modified eagle medium (DMEM) supplemented with 10% fetal bovine serum (FBS), 200 U/mL penicillin, 200 μg/mL streptomycin, and 100 μg/mL hygromycin at 37 °C in a humidified atmosphere containing 5% CO_2. All treatment of PPMOs was performed in OptiMEM medium (Thermo Fisher Scientific, Massachusetts).

Splicing Correction Assay. HeLa 705 cells were seeded in 48-well plates at 30,000 cells/well 24 h before treatment. The culture medium was removed, and the cells were treated with 200 μL of OptiMEM medium containing tested compounds. After 24 h of incubation at 37 °C under 5% CO_2, the medium was removed, and 100 μL of Glo Lysis Buffer (Promega, Wisconsin) was added to lyse cells. Cell lysates were collected into microtubes and centrifuged at 20,000*g* for 10 min at 4 °C to separate insoluble cell debris. Luciferase expression levels were evaluated by mixing 30 μL of cell lysates and 100 μL of a luciferase assay reagent (Promega) followed by measuring the light production using an ARVO SX microplate reader (PerkinElmer, Massachusetts). The antisense activity of each compound was determined by relative light units (RLU) per μg of protein, which was measured by the bicinchoninic acid method (Thermo Fisher Scientific, Massachusetts). Each value of RLU/μg protein shown in the figures was normalized to the value of the vehicle controls.

Flow Cytometry. HeLa 705 cells were seeded in 24-well plates at 100,000 cells/well 24 h before treatment. After the culture medium was removed, the cells were treated with tested compounds in 350 μL of OptiMEM for a specified time. The cells were washed twice with 300 μL of PBS containing 20 U/mL heparin and then treated with 200 μL of trypsin−EDTA (0.05%) for 5 min at 37 °C followed by the addition of 300 μL of culture medium. The cell suspensions were spun down and washed twice with 500 μL of PBS. The obtained cell pellets were resuspended in 500 μL of PBS containing 1% FBS and then analyzed by a BD Accuri C6 Plus flow cytometer (BD Biosciences, New Jersey). The mean fluorescence intensity of each sample is presented as relative to that of **7-F** after 15 h.

Confocal Laser Scanning Microscopy (CLSM). HeLa 705 cells were seeded in multi-well glass-bottom dishes (Matsunami Glass, Osaka, Japan) at 20,000 cells/well 24 h prior to treatment. After the removal of the culture medium, the cells were incubated with 200 μL of OptiMEM containing tested compounds for 6 h at 37 °C under 5% CO_2. The cells were washed with fresh OptiMEM followed by the treatment of Hoechst 33342 and LysoTracker Red (Thermo Fisher Scientific) to stain nuclei and endosomes/lysosomes, respectively. The CLSM observations were performed by using a Nikon A1 confocal laser scanning microscope equipped with a 100× or 40× objective lens at an excitation wavelength of 405 nm for Hoechst 33342, 488 nm for fluorescein, and 561 nm for LysoTracker Red.

Cytotoxicity Assay. HeLa 705 cells were seeded in 96-well plates at 5,000 cells/well 24 h before treatment. The culture medium was removed, and the cells were treated with 100 μL of OptiMEM medium containing tested compounds at 37 °C under 5% CO_2. After 24 h of incubation, 10 μL of a Cell Counting Kit-8 reagent (Dojindo Molecular Technologies, Maryland) was added to each well followed by further incubation. The cell viabilities were determined by normalizing the absorbance at 450 nm of treated cells to that of untreated cells.

■ ASSOCIATED CONTENT

Supporting Information

The Supporting Information is available free of charge at https://pubs.acs.org/doi/10.1021/acs.bioconjchem.2c00199.

Results of the cytotoxicity assay, CLSM observation, HPLC analysis of peptides, and LC−MS analysis of PPMOs (PDF)

■ AUTHOR INFORMATION

Corresponding Author

Yosuke Demizu − *Division of Organic Chemistry, National Institute of Health Sciences, Kanagawa 210-9501, Japan; Graduate School of Medical Life Science, Yokohama City University, Kanagawa 236-0027, Japan; Graduate School of Medicine, Dentistry and Pharmaceutical Sciences, Okayama University, Okayama 700-8530, Japan;* orcid.org/0000-0001-7521-4861; Phone: +81-44-270-6578; Email: demizu@nihs.go.jp; Fax: +81-44-270-6578

Authors

Hiroyuki Takada − *Division of Organic Chemistry, National Institute of Health Sciences, Kanagawa 210-9501, Japan; Graduate School of Medical Life Science, Yokohama City University, Kanagawa 236-0027, Japan;* orcid.org/0000-0001-6650-7902

Keisuke Tsuchiya − *Division of Organic Chemistry, National Institute of Health Sciences, Kanagawa 210-9501, Japan; Graduate School of Pharmacy, Showa University, Tokyo 142-8555, Japan*

Complete contact information is available at: https://pubs.acs.org/10.1021/acs.bioconjchem.2c00199

https://doi.org/10.1021/acs.bioconjchem.2c00199
Bioconjugate Chem. 2022, 33, 1311−1318

Author Contributions

H.T. and Y.D. designed the research and wrote the paper. H.T. and K.T. performed the experiments and analyzed the results. All authors discussed the results and commented on the manuscript.

Notes

The authors declare no competing financial interest.

■ ACKNOWLEDGMENTS

The authors would like to express their deepest appreciation to Dr. Takashi Misawa, Dr. Genichiro Tsuji, and Dr. Yuki Takechi-Haraya (National Institute of Health Sciences) for their help with technical support. This study was supported in part by grants from the Japan Agency for Medical Research and Development (Grant Numbers 22mk0101197j0002, 22fk0210110j0401, 22ak0101185j0301, and 22fk0310506j0701 to Y.D.), the Japan Society for the Promotion of Science and the Ministry of Education, Culture, Sports, Science and Technology (JSPS/MEXT KAKENHI Grant Numbers JP18H05502 and 21K05320 to Y.D.), the Takeda Science Foundation (to Y.D.), the Naito Foundation (to Y.D.), the Sumitomo Foundation (to Y.D.), and the Novartis Foundation (Japan) for the Promotion of Science (to Y.D.). We thank Renee Mosi, PhD, from Edanz (https://jp.edanz.com/ac) for editing a draft of this manuscript.

■ ABBREVIATIONS

Ac_4c, 1-aminocyclobutanecarboxylic acid; Ac_5c, 1-aminocyclopentanecarboxylic acid; Ac_6c, 1-aminocyclohexanecarboxylic acid; Ahx, 6-aminohexanoic acid; Aib, 2-aminoisobutyric acid; Api^{C2Gu}, 4-amino-1-(3-guanidinopropanoyl)piperidine-4-carboxylic acid; CD, circular dichroism; CuAAC, copper-catalyzed azide−alkyne cycloaddition; CPP, cell-penetrating peptide; dAA, α,α-disubstituted α-amino acid; DIPEA, *N*,*N*-diisopropylethylamine; EDTA, ethylenediaminetetraacetic acid; EED, endosomal escape domain; GFP, green fluorescent protein; HPLC, high-performance liquid chromatography; NMP, *N*-methyl-2-pyrrolidone; PBS, phosphate-buffered saline; Pip, PMO internalizing peptide; PMO, phosphorodiamidate morpholino oligomer; PPMO, peptide-conjugated PMO; RLU, relative light unit; TFA, trifluoroacetic acid

■ REFERENCES

(1) Gellman, S. H. Foldamers: A Manifest. *Acc. Chem. Res.* **1998**, *31*, 173−180.
(2) Mándity, I. M.; Fülöp, F. An overview of peptide and peptoid foldamers in medicinal chemistry. *Expert Opin. Drug Discovery* **2015**, *10*, 1163−1177.
(3) Gopalakrishnan, R.; Frolov, A. I.; Knerr, L.; Drury, W. J., III; Valeur, E. Therapeutic Potential of Foldamers: From Chemical Biology Tools To Drug Candidates? *J. Med. Chem.* **2016**, *59*, 9599−9621.
(4) Dougherty, P. G.; Sahni, A.; Pei, D. Understanding Cell Penetration of Cyclic Peptides. *Chem. Rev.* **2019**, *119*, 10241−10287.
(5) Kato, T.; Oba, M.; Nishida, K.; Tanaka, M. Cell-penetrating helical peptides having l-arginines and five-membered ring α,α-disubstituted α-amino acids. *Bioconjugate Chem.* **2014**, *25*, 1761−1768.
(6) Yamashita, H.; Demizu, Y.; Shoda, T.; Sato, Y.; Oba, M.; Tanaka, M.; Kurihara, M. Amphipathic short helix-stabilized peptides with cell-membrane penetrating ability. *Bioorg. Med. Chem.* **2014**, *22*, 2403−2408.
(7) Yamashita, H.; Oba, M.; Misawa, T.; Tanaka, M.; Hattori, T.; Naito, M.; Kurihara, M.; Demizu, Y. A Helix-Stabilized Cell-Penetrating Peptide as an Intracellular Delivery Tool. *ChemBioChem* **2016**, *17*, 137−140.
(8) Potocky, T. B.; Menon, A. K.; Gellman, S. H. Effects of conformational stability and geometry of guanidinium display on cell entry by beta-peptides. *J. Am. Chem. Soc.* **2005**, *127*, 3686−3687.
(9) Bouillère, F.; Thétiot-Laurent, S.; Kouklovsky, C.; Alezra, V. Foldamers containing γ-amino acid residues or their analogues: structural features and applications. *Amino Acids* **2011**, *41*, 687−707.
(10) Nagel, Y. A.; Raschle, P. S.; Wennemers, H. Effect of Preorganized Charge-Display on the Cell-Penetrating Properties of Cationic Peptides. *Angew. Chem., Int. Ed.* **2017**, *56*, 122−126.
(11) Hilinski, G. J.; Kim, Y. W.; Hong, J.; Kutchukian, P. S.; Crenshaw, C. M.; Berkovitch, S. S.; Chang, A.; Ham, S.; Verdine, G. L. Stitched α-helical peptides via bis ring-closing metathesis. *J. Am. Chem. Soc.* **2014**, *136*, 12314−12322.
(12) Oba, M.; Kunitake, M.; Kato, T.; Ueda, A.; Tanaka, M. Enhanced and Prolonged Cell-Penetrating Abilities of Arginine-Rich Peptides by Introducing Cyclic α,α-Disubstituted α-Amino Acids with Stapling. *Bioconjugate Chem.* **2017**, *28*, 1801−1806.
(13) Tian, Y.; Zeng, X.; Li, J.; Jiang, Y.; Zhao, H.; Wang, D.; Huang, X.; Li, Z. Achieving enhanced cell penetration of short conformationally constrained peptides through amphiphilicity tuning. *Chem. Sci.* **2017**, *8*, 7576−7581.
(14) Yokoo, H.; Misawa, T.; Demizu, Y. De Novo Design of Cell-Penetrating Foldamers. *Chem. Rec.* **2020**, *20*, 912−921.
(15) Copolovici, D. M.; Langel, K.; Eriste, E.; Langel, Ü. Cell-penetrating peptides: design, synthesis, and applications. *ACS Nano* **2014**, *8*, 1972−1994.
(16) Kurrikoff, K.; Vunk, B.; Langel, Ü. Status update in the use of cell-penetrating peptides for the delivery of macromolecular therapeutics. *Expert Opin. Biol. Ther.* **2021**, *21*, 361−370.
(17) Moulton, H. M.; Nelson, M. H.; Hatlevig, S. A.; Reddy, M. T.; Iversen, P. L. Cellular uptake of antisense morpholino oligomers conjugated to arginine-rich peptides. *Bioconjugate Chem.* **2004**, *15*, 290−299.
(18) Abes, S.; Moulton, H. M.; Clair, P.; Prevot, P.; Youngblood, D. S.; Wu, R. P.; Iversen, P. L.; Lebleu, B. Vectorization of morpholino oligomers by the (R-Ahx-R)4 peptide allows efficient splicing correction in the absence of endosomolytic agents. *J. Controlled Release* **2006**, *116*, 304−313.
(19) Wu, R. P.; Youngblood, D. S.; Hassinger, J. N.; Lovejoy, C. E.; Nelson, M. H.; Iversen, P. L.; Moulton, H. M. Cell-penetrating peptides as transporters for morpholino oligomers: effects of amino acid composition on intracellular delivery and cytotoxicity. *Nucleic Acids Res.* **2007**, *35*, 5182−5191.
(20) Gait, M. J.; Arzumanov, A. A.; McClorey, G.; Godfrey, C.; Betts, C.; Hammond, S.; Wood, M. J. A. Cell-Penetrating Peptide Conjugates of Steric Blocking Oligonucleotides as Therapeutics for Neuromuscular Diseases from a Historical Perspective to Current Prospects of Treatment. *Nucleic Acid Ther.* **2019**, *29*, 1−12.
(21) Wolfe, J. M.; Fadzen, C. M.; Holden, R. L.; Yao, M.; Hanson, G. J.; Pentelute, B. L. Perfluoroaryl Bicyclic Cell-Penetrating Peptides for Delivery of Antisense Oligonucleotides. *Angew. Chem., Int. Ed.* **2018**, *57*, 4756−4759.
(22) Kang, S. H.; Cho, M. J.; Kole, R. Up-regulation of luciferase gene expression with antisense oligonucleotides: implications and applications in functional assay development. *Biochemistry* **1998**, *37*, 6235−6239.
(23) Abes, R.; Moulton, H. M.; Clair, P.; Yang, S. T.; Abes, S.; Melikov, K.; Prevot, P.; Youngblood, D. S.; Iversen, P. L.; Chernomordik, L. V.; et al. Delivery of steric block morpholino oligomers by $(R\text{-}X\text{-}R)_4$ peptides: structure-activity studies. *Nucleic Acids Res.* **2008**, *36*, 6343−6354.
(24) Lehto, T.; Castillo Alvarez, A.; Gauck, S.; Gait, M. J.; Coursindel, T.; Wood, M. J. A.; Lebleu, B.; Boisguerin, P. Cellular trafficking determines the exon skipping activity of Pip6a-PMO in mdx skeletal and cardiac muscle cells. *Nucleic Acids Res.* **2014**, *42*, 3207−3217.

https://doi.org/10.1021/acs.bioconjchem.2c00199
Bioconjugate Chem. 2022, 33, 1311−1318

(25) Fadzen, C. M.; Holden, R. L.; Wolfe, J. M.; Choo, Z. N.; Schissel, C. K.; Yao, M.; Hanson, G. J.; Pentelute, B. L. Chimeras of Cell-Penetrating Peptides Demonstrate Synergistic Improvement in Antisense Efficacy. *Biochemistry* **2019**, *58*, 3980−3989.
(26) Youngblood, D. S.; Hatlevig, S. A.; Hassinger, J. N.; Iversen, P. L.; Moulton, H. M. Stability of cell-penetrating peptide-morpholino oligomer conjugates in human serum and in cells. *Bioconjugate Chem.* **2007**, *18*, 50−60.
(27) Lönn, P.; Kacsinta, A. D.; Cui, X. S.; Hamil, A. S.; Kaulich, M.; Gogoi, K.; Dowdy, S. F. Enhancing Endosomal Escape for Intracellular Delivery of Macromolecular Biologic Therapeutics. *Sci. Rep.* **2016**, *6*, 32301.
(28) Shabanpoor, F.; Gait, M. J. Development of a general methodology for labelling peptide-morpholino oligonucleotide conjugates using alkyne-azide click chemistry. *Chem. Commun.* **2013**, *49*, 10260−10262.

https://doi.org/10.1021/acs.bioconjchem.2c00199
Bioconjugate Chem. 2022, 33, 1311−1318